Magnetocrystalline interactions in $MnCr_2O_4$ spinel

E. Winkler,[1,*] S. Blanco Canosa,[2] F. Rivadulla,[2] M. A. López-Quintela,[2] J. Rivas,[3] A. Caneiro,[1] M. T. Causa,[1] and M. Tovar[1]

[1]*Centro Atómico Bariloche, S. C. de Bariloche, 8400 Rio Negro, Argentina*

[2]*Departamentos de Química-Física, Universidad de Santiago de Compostela, 15782 Santiago de Compostela, Spain*

[3]*Departamentos Física Aplicada, Universidad de Santiago de Compostela , 15782 Santiago de Compostela, Spain*

(Received 24 April 2009; revised manuscript received 30 June 2009; published 15 September 2009)

In this work we present a magnetic, structural, and electron spin resonance (ESR) study of the geometrically frustrated $MnCr_2O_4$ spinel in an extended range of T (2–1000 K). At the lowest temperature ($T<18$ K) the ESR lineshape is compatible with the coexistence of spiral and ferrimagnetic spin ordering. Above T_C (≈ 41 K), magnetic susceptibility (χ) and ESR intensity coincide with each other showing the typical behavior of a ferrimagnet. From the $\chi(T)$ vs T dependence, absolute values for the three exchange constants J_{MnCr}, J_{CrCr}, and J_{MnMn} were determined. Our results indicate that (i) these values are approximately independent of T, (ii) the antiferromagnetic direct Cr-Cr exchange is the main interaction, and (iii) J_{MnMn} is indeed not negligible as compared with J_{MnCr} and J_{CrCr}. One noticeable anomaly in the temperature dependence of the ESR linewidth is observed at $T \approx 450$ K. This behavior is accounted by a 30% variation in the extrapolated high-temperature linewidth and it is attributed to a crystalline distortion not reported previously. Experiments of high-temperature x-ray diffraction allowed us to associate this distortion to a deformation of the oxygen sublattice. ESR and x-ray results are both compatible with a more symmetric high-temperature structure.

DOI: 10.1103/PhysRevB.80.104418 PACS number(s): 75.30.Et, 76.30.−v

I. MOTIVATION

In spite of the wide research developed in transition-metal oxides these materials continue to attract the attention of the condensed matter community. This stage is explained by the great variety of unconventional phenomena displayed by these materials, which are imparted by the outer d electrons of the transition-metal ions.[1] In particular, the AB_2O_4 oxides with spinel structure have rich phase diagrams due to the correlations between their magnetic, electrical, and structural properties.[2] Recent experiments have shown that the family of chromite spinel ACr_2O_4 presents important electric (A =Mn,Co) (Refs. 3–5) and elastic (A=Hg) (Refs. 6 and 7) response to external magnetic fields. The magnetodielectric and magnetoelastic coupling develops at low temperature when the system presents a magnetic frustrated order state. In the former case the magnetization reversal by means of applied magnetic field induced a reversal of the electric polarization. In the second case $HgCr_2O_4$, the oxide presents a structural change from cubic to orthorhombic at the magnetic transition temperature. By an applied magnetic field the lattice constant expand and the geometric frustration is relived. These attributes, coupled with the great flexibility of the spinel crystalline structure to host different cations shows the great potential of these materials to designs devices with specific characteristic and tune a particular property to a temperature, pressure, or field condition.[8]

In the present paper, we analyze the high-temperature magnetic and structural properties of the cubic spinel $MnCr_2O_4$, where $Mn^{2+}(3d^5, t_{2g}^3 e_g^2)$ occupies the tetrahedral A sites and $Cr^{3+}(3d^3, t_{2g}^3 e_g^0)$ occupies the B sites with octahedral coordination. The spatial arrangement of the B sites (pyrochlorelike) leads to a very high degree of magnetic frustration when the nearest-neighbor interactions are antiferromagnetic (AFM). This geometrical frustration is the origin of the low T_C and unusual magnetic ordering in spite of the strong direct-exchange energies observed ($\Theta_{CW}/T_C > 10$).[9–11] $MnCr_2O_4$, besides the ferrimagnetic order at $T_C \approx 41-51$ K, develops a short-range spiral order at low temperature, $T_F = 14-18$ K.[12,13] On the other hand, the ferrimagnetic ordering temperature increases substantially when Cr^{3+} is replaced by ions with e_g electrons; for example $MnFe_2O_4$ presents $T_C \sim 573$ K,[2] suggesting that the magnetic frustration is released through the superexchange B^{3+}-O-A^{2+} path. These evidences support the assumption of a dominant B^{3+}-B^{3+} over the B^{3+}-O-A^{2+} interaction, when the octahedral site ion has empty e_g orbital. If this effect is verified, the Cr, V, or Ti spinels (with e_g^0 orbital) could be used as simple models to study the evolution of the direct-exchange interaction and the metal-insulator transition in Mott insulators. This study may be achieved decreasing the metal-metal distance along isostructural series changing the A site ions.[14] *Ab initio* calculations suggested that the direct Cr-Cr exchange constant J_{CrCr} could be over three times larger than the superexchange Cr-O-Mn constant J_{MnCr}, but an experimental confirmation is still lacking.[14]

From the susceptibility, $\chi(T)$, measured in the paramagnetic range, we have obtained absolute values for the exchange constants showing that the direct Cr-Cr exchange is indeed the dominant interaction. From ESR we have found a crystalline distortion not reported previously manifested as an anomaly in the linewidth behavior. Contrarily to the results in other oxides this distortion could not be associated to changes in χ (T).[15] Experiments of x-ray diffraction in the same temperature range allowed us to relate the linewidth anomaly to deformations of the oxygen sublattice. Our results show the extreme sensitivity of the ESR spectroscopy to unveil changes in the magnetic anisotropy of local-moment systems which are difficult to detect by conventional techniques.

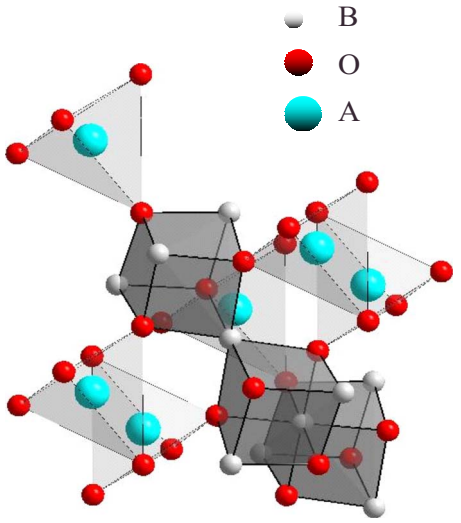

FIG. 1. (Color online) Distorted crystal structure of AB_2O_4 spinel, where the O ions are shifted into the body diagonal direction.

II. SAMPLE DESCRIPTION AND EXPERIMENTAL DETAILS

The spinel oxides, AB_2O_4, are characterized by a cubic unit cell with F*d*-3*m* symmetry. In the ideal structure, the O^{2-} ions form a *fcc* cubic lattice where the cations occupy tetrahedral (A) and octahedral (B) interstices. The distorted structure is obtained from the ideal one by a shift of all O ions in the body diagonal direction in such a way that all A-O distances are equal[16] (see Fig. 1). The ion position are then determined by only one parameter, u, that in the ideal case is $u=0.25$.

Single-phase polycrystalline $MnCr_2O_4$ was synthesized by solid-state reaction of Cr_2O_3 and MnO in air at 1100 °C for 48 h with an intermediate grinding. Powder x-ray diffraction data were collected on a Philips PW1700 diffractometer using Cu Kα radiation and a graphite monochromator. High-temperature x-ray diffraction data were collected by spreading the sample onto a resistively heated platinum ribbon in an Anton Paar HTK-10 chamber coupled to the diffractometer. Structural parameters were derived from x-ray diffraction patterns by Rietveld analysis with the program Rietica. Magnetic properties were studied in the range 5–1000 K. For $T>250$ K we have used a homemade Faraday balance magnetometer and for $T<300$ K the measurements were performed with a commercial SQUID magnetometer. From the magnetic susceptibility $\chi(T)$ we have obtained the paramagnetic (PM) contribution $[\chi(T)\equiv\chi_{PM}(T)]$; since we have estimated that the Van-Vleck susceptibility contribution χ_{VV} (that should be included in others Cr^{3+} compounds)[17] and the diamagnetic contribution χ_d are negligible in the ferrimagnetic $MnCr_2O_4$ oxide.

The ESR spectra were recorded with a Bruker ESP300 spectrometer operating at $\nu\approx9.5$ GHz and equipped with special cavities to cover the temperature range from 2 to 1000 K. From the ESR spectra in the paramagnetic regime, we derived three parameters: the resonance field (H_r), the linewidth (ΔH), and the ESR intensity (I_{ESR}). From H_r the gyromagnetic factor $g=g_0+\varepsilon$ was derived, where $g_0=2.0023$ is the free-electron g and the g shift, ε, depends (for 3*d* ions) on the ratio between spin-orbit and crystal-field interactions. The linewidth is a measurement of the spin-relaxation mechanism and could be theoretically estimated considering the spin Hamiltonian of the system.[18] For a derivative spectrum, ΔH is measured as the distance between its peaks. The spectrum intensity is the area under the absorption curve, and results proportional to dc susceptibility when all the magnetic ions contribute to the resonance and χ_{VV}, $\chi_d \ll \chi_{PM}$. This area can also be approximated by $I_{ESR} \propto h(\Delta H)^2$ where h is the height between peaks and the proportionality constant depends of the lineshape (3.63, for Lorentzians).

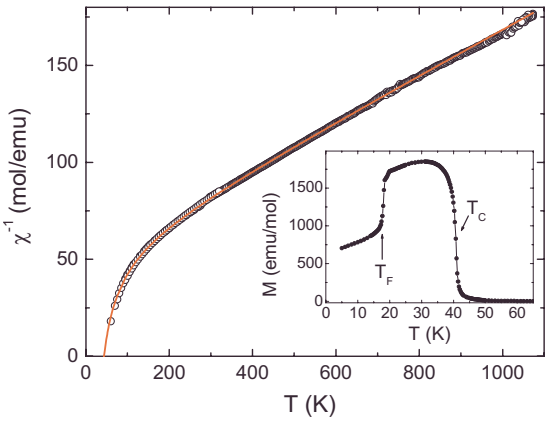

FIG. 2. (Color online) Temperature variation in χ^{-1}. The solid line corresponds to the fitting curve to Eq. (1) with the fitting parameter presented in Table I. The inset shows a detail of the low-temperature magnetization measured with $H=100$ Oe. The ferrimagnetic transition, T_C and the helical order temperature T_F are marked with arrows.

III. MAGNETIZATION

Magnetization measurements $[M(T)]$, at low temperature were performed with an applied field of $H=100$ Oe. In the inset of Fig. 2 we show the temperature dependence of the magnetization where two transition at 41 and 18 K are clearly manifested. This anomalies are in agreement with the long-range ferrimagnetic transition (T_C) and the helical order temperature (T_F), respectively, determined from neutron diffraction experiment.[12,19]

For $T>T_C$, $M(T)$ was measured with magnetic fields up to 1 T finding a linear dependence: $M(T)=\chi(T)H$. We have observed that $\chi^{-1}(T)$ follows the hyperbolic behavior characteristic of ferrimagnets[2,20] described by

$$\chi^{-1}(T)=[(T-\Theta)/C]-[\xi/(T-\Theta')] \quad (1)$$

where the first term is the hyperbole high-T asymptote that has a Curie-Weiss (CW) form. We fitted the experimental data to Eq. (1) and the resulting parameter values are presented in Table I. From these values we extrapolated the critical temperature obtaining $T_C=43(9)$ K (see Fig. 2) in agreement with the measured low-temperature transition (inset Fig. 2).

TABLE I. Ferrimagnetic parameters obtained from the fitting of the susceptibility with Eq. (1). At the bottom of the table we have included the exchange constant obtained from Θ, Θ', ξ values and mean-field coefficients.

C (emu-K/mol)	Θ (K)	Θ' (K)	ξ (mol-K/emu)
8.57(2)	−462(4)	6(2)	2180(64)
$2J_{MnMn}/k_B$ (K)	$2J_{CrCr}/k_B$ (K)	$2J_{MnCr}/k_B$ (K)	
−10.4(5)	−48.9(2)	−16.2(1)	

In order to describe the PM behavior in terms of a Weiss mean-field (MF) model we followed the Lotgering paper[16] where the magnetic lattice is subdivides in two Mn^{2+} and four Cr^{3+} sublattices. The lattice subdivision is performed in order to a given ion have not nearest-neighbors (nn) interaction with ions of its own sublattice. Therefore for this calculation only nn interactions between ions of different sublattice are included. In the paramagnetic phase, the Mn^{2+} and Cr^{3+} magnetization are given by:

$$M_{Mn} = [C_{Mn}/T][H - (1/2)\lambda_{MnMn}M_{Mn} - 2\lambda_{MnCr}M_{Cr}] \quad (2)$$

$$M_{Cr} = [C_{Cr}/T][H - \lambda_{MnCr}M_{Mn} - (3/2)\lambda_{CrCr}M_{Cr}] \quad (3)$$

where C_{Cr}, and C_{Mn} are the free-ion Curie constant for high-spin $Cr^{3+}(S=3/2)$ and Mn^{2+} $(S=5/2)$. The MF coefficients λ_{ij} are given by:[20]

$$\lambda_{ij} = [n_j k_B/N_{Av}\mu_B^2][z_{ij}(2J_{ij}/k_B)/g_i g_j] \quad (4)$$

where g_i is the g factor of the i ion, J_{ij} is the exchange coupling between ions belonging to two different $(i \neq j)$ sublattices, z_{ij} is the number of j-nn ions, and N_{Av}/n_j is the number (per mol) of j ions in the corresponding sublattice. For spinel $z_{Cr\text{-}Cr}=2$, $z_{Mn\text{-}Cr}=3$, $z_{Mn\text{-}Mn}=4$, and $n_j=2$ for all j.

Solving the coupled Eqs. (2) and (3), we obtain the total magnetization per mol of the compound,

$$M = [M_{Mn} + 2M_{Cr}] = \chi(T)H. \quad (5)$$

Comparing Eqs. (1) and (5), we found the following relations between the fitted parameters and the free-ion Curie constants and MF coefficients

$$C = C_{Mn} + 2C_{Cr} \quad (6)$$

$$\Theta = -(1/C)[(1/2)C_{Mn}^2\lambda_{MnMn} + 3C_{Cr}^2\lambda_{CrCr} + 4C_{Mn}C_{Cr}\lambda_{CrMn}] \quad (7)$$

$$\Theta' = -(C_{Mn}C_{Cr}/C)[\lambda_{MnMn} + (3/2)\lambda_{CrCr} - 4\lambda_{CrMn}] \quad (8)$$

$$\xi = (2C_{Mn}C_{Cr}/C^3)[-(1/2)C_{Mn}\lambda_{MnMn} + (3/2)C_{Cr}\lambda_{CrCr} + (C_{Mn} - 2C_{Cr})\lambda_{CrMn}]^2 \quad (9)$$

From the theoretical C_{Mn} and C_{Cr} values, for a normal spinel result $C=8.0474$ emu-K/mol, which is some lower than the fitted value $C=8.57(2)$emu-K/mol (see Table I). From Eq. (7)–(9) and using the fitted C, Θ, Θ' and ξ values, we obtained the AFM exchange constants J_{ij} that are presented in Table I. Here we have retained explicitly the factor 2 in Eq. (4) which corresponds to our choice[20] for the Heisenberg Hamiltonian: $H_{ex}=-2\ JS_i(\Sigma'_{nn}S_j)$ that differs from the definition used by other authors.[21]

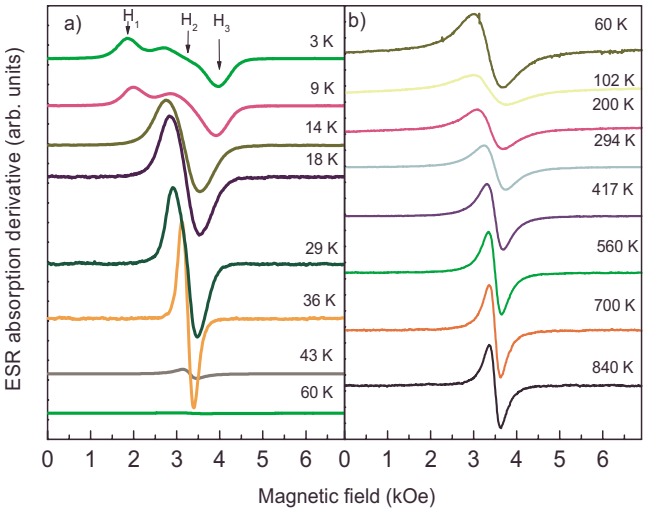

FIG. 3. (Color online) ESR absorption derivative spectra of the $MnCr_2O_4$ spinel for several temperatures. Notice that the ESR spectra at T_C and T_F show important changes.

Our result for the Cr-Cr interaction is in excellent agreement with the value derived in Ref. 10 from the experimental CW temperature of the AFM $ZnCr_2O_4$. The ratio $R = J_{CrCr}/J_{CrMn} = 3.02$ (see Table I), evidences that direct overlapping of $d-d$ orbital is the main mechanism for exchange in our case, been more efficient that $d-p$ superexchange as was observed in V spinels[22] as well as in other Cr^{3+} oxides.[2,23] Besides, the R value is in agreement with that reported by Blanco-Canosa *et al.*[14] based in a total energy calculation fitted to a Heisenberg model. Regarding to the Mn-Mn interaction, notice that we have included only nearest-neighbor interaction that is the strongest one.[16,24] Tristan *et al.*,[25] for the $MnAl_2O_4$ spinel, obtained a much lower average value for J_{MnMn} considering 28 neighbors at different distances and several indirect exchange paths. We have also analyzed the Edwards[26] experiments performed also on $MnAl_2O_4$. Although Al^{3+} is not magnetic $\chi^{-1}(T)$ showed a ferrimagnetic convexity at low temperature reflecting the presence of a few percent of inverted spinel, with $\approx 5\%$ of Mn in the B sites. We fitted the data with Eq. (1) and we have obtained for Mn^{2+}-Mn^{2+} nn interaction: $J_{MnMn}/k_B = -13.8$ K. The small increases of this value with respect to the J_{MnMn}/k_B showed in Table I for $MnCr_2O_4$ is consistent with the decreases of the lattice dimensions pointed out by Edwards.[26]

IV. ELECTRON SPIN RESONANCE

In Fig. 3 we show representative $MnCr_2O_4$ ESR spectra taken at different temperatures. In the PM range, the resonance consists of a single (without structures) Lorentzian

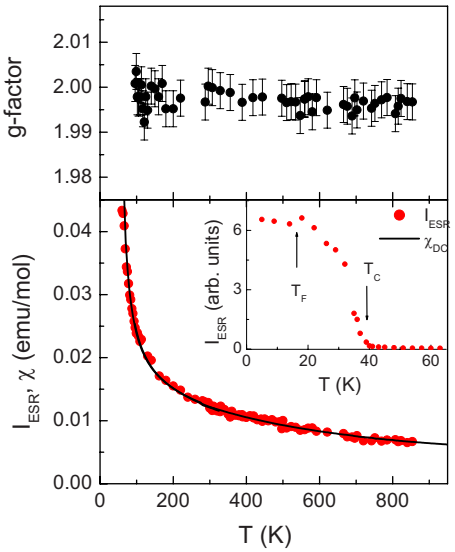

FIG. 4. (Color online) The upper graph shows the g factor as a function of the temperature. The lower graph shows the temperature dependence of the magnetic susceptibility and the ESR intensity normalized to a reference compounds. The inset shows I_{ESR} vs T around the ferrimagnetic transition temperature.

line centered at an essentially constant H_r=3370 Oe. From H_r, we have obtained $g=(h\nu)/(\mu_B H_r)=1.994(3)$ [see Fig. 4(a)]. In magnetic materials with relatively high T_C, the exchange interaction dominates over the Zeeman interaction and even though two different magnetic species are present only one line is observed. In this case the expected g is an average of the individual g, given by:[27]

$$g=[g_{Mn^{2+}}W_{Mn}+g_{Cr^{3+}}W_{Cr}]/[W_{Mn}+W_{Cr}] \qquad (10)$$

where the factors $W_{Mn}=N_{Mn}S_{Mn}(S_{Mn}+1)$, $W_{Cr}=N_{Cr}S_{Cr}(S_{Cr}+1)$, and $N_{Mn,Cr}$ is the relative concentration of Mn^{2+} and Cr^{3+}, respectively. Using $g_{Mn^{2+}}=2.001$ and $g_{Cr^{3+}}=1.978$,[9,28] we obtain $g=1.990$ in good agreement with the experimental result. Notice that in Eq. (10) a normal spinel structure was assumed. Then the agreement with the experimental g value supports this hypothesis.

When the temperature decreases the intensity, $I_{ESR} \propto h\Delta H^2$, increases monotonically, as is observed in Fig. 4(b). This behavior abruptly changes when T_C is approached: I_{ESR} starts to increase at higher rates and, at the same time, H_r shifts to lower magnetic fields and ΔH broadens up. These experimental facts are associated to the presence of internal fields proportional to the spontaneous magnetization that increases rapidly for temperatures close to T_C.[29] Below T_C, the spins equilibrium state changes and depends on the H direction and magnitude. As a consequences of strong exchange and anisotropy fields, different resonant modes appear. A detailed ESR study in the ordered state requires monocrystalline samples and ESR experiments performed with several different frequencies. Nevertheless, as we explain below, changes in the ESR lineshape may be associated to neutron experiment characteristic temperatures.

The ESR spectrum presents important changes at $T \sim 18$ K (see Fig. 3). Important departures from Lorentzian shape are manifested and secondary peaks become visible.

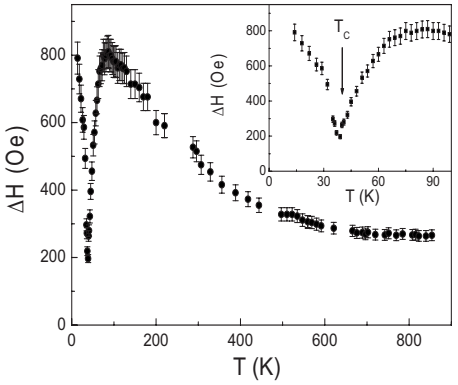

FIG. 5. Temperature variation in ΔH. Inset: we show in detail the temperature region around T_C

This kind of lineshape is compatible with powder spectra of ferromagnets that could be modeled[30] assuming a distribution of anisotropy fields. The magnetic anisotropy is related to the local internal magnetic field which is modified when the system develops the ferrimagnetic spiral order at T_F. In Fig. 3(a) the characteristic fields (H_1, H_2, and H_3) are signaled with arrows and correspond to the resonance absorption when the magnetic field is along one of the anisotropy axis.[30] This result is consistent with the neutron diffraction study reported in Ref. 12. In the mentioned work it is found that, below T_F, ferrimagnetic long-range order and short-range spiral order coexist. The propagation vector of the spiral component is along the [110] direction and the ferrimagnetic order present an easy axis along the [1–10] direction. As can be seen the described magnetic order defined three (orthogonal) main anisotropy directions consistent with the ESR powder spectra feature.

In Fig. 4(b) the temperature dependence of $I_{ESR}(T)$ and $\chi(T)$ are shown for $T>T_C$. As it is expected for a compound where all the spins contribute to the resonance, I_{ESR} is proportional to the dc susceptibility in all the PM range. A perfect overlap between both experimental curves is obtained when I_{ESR} is normalize to a reference compounds as explained in Ref. 31.

The inset of Fig. 4(b) shows a detail of the I_{ESR} at the low temperature range, where a remarkable growing of the intensity at T_C is observed. This is associated to the sudden increases in the magnetization below T_C. The line intensity grows when T diminishes but at $T \sim T_F$, in coincidence with the changes in the ESR lineshape, I_{ESR} stops to increase. Similar features were observed in M vs T curves measured with different applied fields.[3]

Figure 5 shows the temperature dependence of the linewidth, $\Delta H(T)$. When the temperature increases $\Delta H(T)$ increases, goes through a maximum at $T \sim 85$ K and then presents a minimum at T_C. The temperature dependence of ΔH shows different forms associated to the dominant magnetic interactions. For exchange coupled paramagnets it was established that:[31]

$$\Delta H(T)=[\chi_S(T)/\chi(T)]\Delta H_\infty \qquad (11)$$

where $\chi_S(T)=C/T$ is the free-ion susceptibility. The factor ΔH_∞ is the high-temperatures extrapolated value of ΔH, in

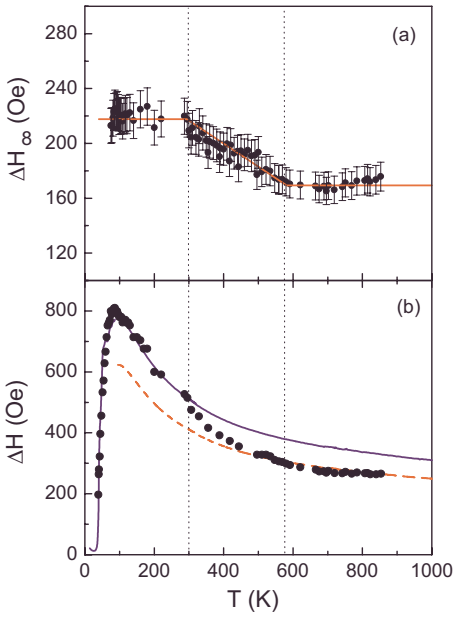

FIG. 6. (Color online) (a) Temperature dependence of ΔH_∞. Notice that above $T \approx 550$ K and below $T \approx 300$ K ΔH_∞ is constant. (b) ΔH temperature dependence in the PM range, with solids lines (dash line) we show the estimated $\Delta H(T)$ obtained from Eq. (11), using the value $\Delta H_\infty = 219$ Oe ($\Delta H_\infty = 172$ Oe).

this limit $\chi(T)$ approaches the $\chi_S(T)$ behavior. Usually ΔH_∞ is determined as the adjustable parameter to fit the experimental data. Theoretical determinations of ΔH_∞, in the general framework of the spin-relaxation theory, involve microscopic parameters associated with the spin Hamiltonian of the system. Linewidth estimations for different crystalline lattices including isotropic and anisotropic interactions has been reported.[15,32–36] Although specific calculations for the spinel structure is still lacking, a qualitative analysis will be presented below.

In order to obtain the constant ΔH_∞ from Eq. (11), we plot in Fig. 6(a) the product $[\Delta H(T)T\chi(T)]/C$ vs T. We observe that ΔH_∞ is *not constant* as would be in an ideal PM compound. Instead it changes from $\Delta H_\infty \approx 172(6)$ Oe for $T > 550$ K to $\Delta H_\infty \approx 219(7)$ Oe for $T < 300$ K, showing, in the intermediate region, a monotonous evolution between this two values. This feature is similar to behavior reported in manganites around the Jahn-Teller distortion.[15]

Replacing these values in Eq. (11), the temperature dependence of ΔH was estimated and compared with the experimental data in Fig. 6(b). A departure of Eq. (11) is clearly observed in the region 300–550 K. Instead, the experimental data show an excellent agreement with Eq. (11) for $T < 300$ K where $\Delta H_\infty = 219$ Oe, and for $T > 500$ K where $\Delta H_\infty = 172$ Oe.

In order to understand the temperature evolution of the ΔH_∞ we have considered the effect of the different interactions into the linewidth. ΔH_∞ depends on the anisotropic (isotropic) spin-spin interactions that contribute to the broadening (narrowing) of the ESR lines, resulting $\Delta H_\infty \propto E_{AI}^2/E_{IE}$.[18] The main isotropic contribution (E_{IE}) comes from the isotropic exchange between near-neighbors spins. The anisotropic interactions (E_{AI}) are related to specific characteristics of the crystalline lattice. Even though dipolar interactions are always present, other E_{AI} mechanisms would be predominant in magnetic compounds with high T_C.[15,32] Taking in account that the susceptibility behavior, with a ferrimagnetic curve, was fitted with one single set of parameters, it is a good approximation to consider that the main spin-spin interaction E_{IE} does not change in all the PM range. Therefore, the observed anomalies in ΔH_∞ are most likely a consequence of changes in E_{AI}. This, in turn, suggests that a crystalline distortion would develop between 300 and 550 K from a distorted to a more symmetric high-temperature lattice with $E_{AI}(300\ \text{K}) > E_{AI}(550\ \text{K})$. Structural changes in the 300/550 K range were not reported previously for $MnCr_2O_4$. Then, in order to elucidated wether the observed anomalies in ΔH_∞ can be related with changes in the structure, we performed high-temperature x-ray powder diffraction and refined the structural parameters.

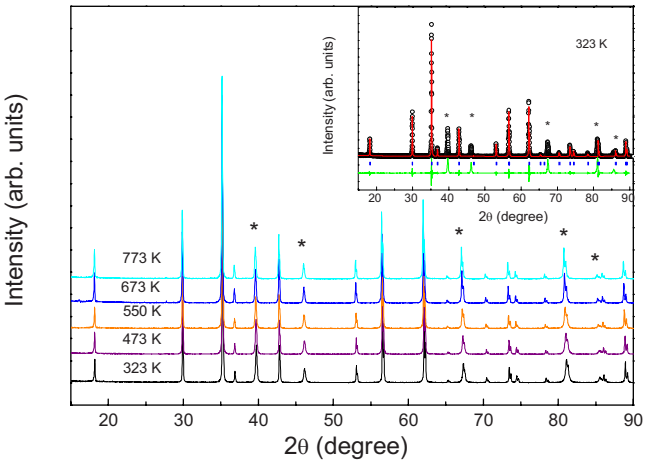

FIG. 7. (Color online) $MnCr_2O_4$ x-ray diffraction patterns for several temperatures. The stars mark the position of the Pt holder peaks. The inset shows a representative Rietveld refinement; the plot includes x-ray diffraction intensity (symbols), the corresponding fit (solid line) and their difference (bottom solid line), and the expected Bragg peaks (vertical bars).

V. CRYSTALLOGRAPHIC PROPERTIES

The x-ray diffraction patterns were measured for several temperatures from room temperature to 773 K. In Fig. 7 some representative powder diffraction patterns are shown, where the diffraction peaks of the platinum x-ray holder are indicated. From Rietveld refinement we have obtained the lattice parameter for the cubic Fd-3m spinel structure, resulting $a = 8.449(2)$Å at 323 K, consistent with values reported in the literature for $T = 295$ K: $a = 8.410(2) - 8.450(4)$Å for different grain size.[13,37,38] In the inset of Fig. 7 we show a representative Rietveld refinement at $T = 323$ K.

The thermal evolution of the a lattice constant and the u parameter derived from the Rietveld refinements are shown in Fig. 8. The lattice parameter grows monotonously from 8.450(0.002)Å at room temperature to 8.4651(0.001)Å at 750 K [Fig. 8(a)]. On the other hand the u parameter presents an abrupt change in the 400–600K temperature range [see Fig. 8(b)]. In this temperature range it is observed that u

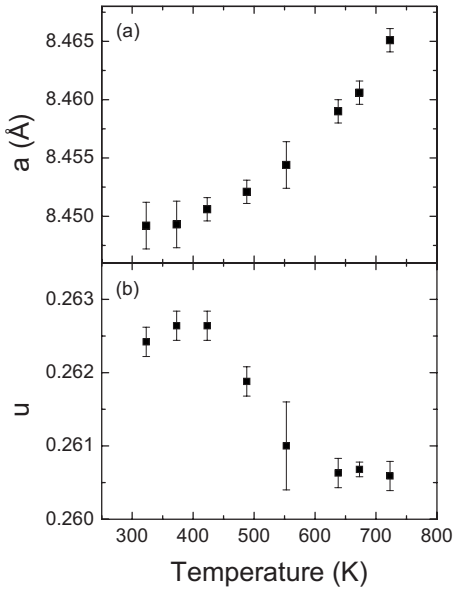

FIG. 8. Thermal evolution of the a lattice constant and the u parameter derived by means of the Rietveld method.

changes from $u \sim 0.2625$ at low temperature ($T < 400$ K); to $u \sim 0.2606$ at high-temperature ($T > 550$ K). As we mentioned above, the u parameter measures the anion sublattice distortion from cubic close packing where $u = 0.25$. Therefore from our measurements it is noteworthy that, when the temperature increases the u parameter decreases toward the value of the undistorted octahedral. This result implies that the system evolves toward a more symmetric high-temperature structure which is in agreement with the decrease in the high-temperature anisotropy energy found by ESR spectroscopy.

Studies of the crystalline evolution at high temperature in normal spinel are lacking in the literature. However, there are some studies of the pressure response of the spinel crystalline structure.[39,40] It was found that when the pressure increases the normal spinel evolves toward a more symmetric structure, i.e., u decreases with pressure and approaches to nondistorted ideal structure where $u = 0.25$.[39] Similar behavior it is also observed in Mn perovskite with Jahn-Teller (JT) distortion. For example, $LaMnO_3$ presents an important JT distortion at room temperature; when T increases, the distortion diminishes and finally at $T > 725$ K is suppressed and the crystalline structure corresponds to the pseudocubic O phase. It was also established that, the Jahn-Teller distortion can be also suppressed by the pressure.[41,42] However, in spite of this similar behavior, while in the perovskite the changes in the crystal structure modifies as much the Curie-Weiss temperature as ΔH_∞, in the spinel oxide only ΔH_∞ changes through the distortion. This important difference can be understood taking into account that in the manganite the superexchange Mn-O-Mn interaction that governs the magnetic properties is also influenced by the changes in the crystal structure that modify the MnO_6 octahedral tilting and the Mn-O distance. Therefore the exchange parameter changes with T, which is reflected in the nonconstant behavior of Θ. Instead, in the spinel oxide the distortion involves the anion sublattice and we have shown that the main interaction is the Cr-Cr direct exchange which does not show a significant modification through the transition.

VI. CONCLUSIONS

We have presented an experimental study of the magnetic and structural properties of $MnCr_2O_4$ a typical example of frustrated spin system. Our study was focused on the high-temperature paramagnetic range. From the temperature dependence of the magnetic susceptibility we derived the values for the three nearest-neighbor exchange constants: J_{MnMn}, J_{CrCr}, and J_{MnCr}. Our results confirm that the coupling between nearest-neighbor Cr^{3+} ions is the main interaction and has antiferromagnetic character. This is a clear indication that AFM direct exchange, involving d orbital overlapping, predominates over the FM-90° superexchange mediated by O^{2-}-p orbital. On the other hand, we have obtained a relatively large value for the Mn-Mn superexchange interaction (see Table I), concluding that, compared with J_{MnCr} and J_{CrCr}, J_{MnMn} would not be negligible as it was considered in former theoretical studies of the ground-state spin configuration.[43] Our result is a contribution to theoretical discussions presented in more recent papers[44,45] that draw attention to the possible importance of the AA interaction in spinel systems with magnetic ions on both, A and B, sites. Systematic measurements of $\chi(T)$ vs T in the high-temperature paramagnetic region, enable to determine absolute values for the exchange constants and show to be an appropriated technique for the study of spinel compounds families. Subtle changes in the exchange constants could originate the different kinds of magnetic order found at the lowest temperatures.

The analysis of the ESR results are greatly based on the perfect matching between susceptibility and ESR intensity. From this fact, we conclude that Eq. (1) describes, with a single set of parameters, the behavior of the resonant spins. Then, as isotropic exchange interactions remains unchanged in all the experimental T range, the less intense anisotropic interactions would be responsible for the 30% decrease in ΔH_∞. Later, crystallographic experiments allowed us to associate the ESR anomaly with variations in the oxygen positions (change of 1% in u) keeping the same overall Fd-3m structure with a monotonous increasing of the parameter a. The major changes would be associated to Mn-O bonds that are less stiff than Cr-O ones.[39] Then, through the transition, the Cr-Cr distances would remain essentially unchanged an so the direct-exchange constant J_{CrCr}. Regarding the absolute values of ΔH_∞, is interesting the comparison with $LaMnO_3$ that also presents a linewidth anomaly. In the more symmetric high-temperature phase, $\Delta H_\infty \sim 2500$ Oe was measured.[15] This value is much larger than $\Delta H_\infty \sim 172$ Oe obtained for $MnCr_2O_4$. On the one hand, the exchange narrowing effect is more effective in spinels due to the higher J values since $\Theta(MnCr_2O_4)/\Theta(LaMnO_3) \sim 2$. On the other hand, the strong antysymmetric exchange arising from Dzialoshinski-Moriya mechanism, that is the main contribution in perovskites, is absent in cubic spinels.[46] Therefore, isotropic and anisotropic interactions contribute to en-

large ΔH_∞ for manganites as compared with spinel compounds. The agreement with experimental results for both structures support the theoretical framework used in this paper.

Finally, we want to highlight the noticeable sensitive of the ESR spectroscopy to detect magnetic transitions and structural distortions. The ESR experiment is sensitive to isotropic and anisotropy interactions and both effects distinguished by means of simultaneous measurements of the ESR intensity and ESR linewidth as a function of T. Small devia tion of ΔH_∞ from an expected constant behavior are easily detected. These anomalies clearly signal the presence of additional crystalline distortions even if the overall crystallographic phase remains unchanged.

The work was supported by PICTR 20770/04 and PICT00829/06, U.N.C. Grant No. 882/07, and CONICET Argentina PIP Grant No. 5250/03. S.B.C. acknowledges FPU grant from the Ministery of Science and Technology of Spain.

*winkler@cab.cnea.gov.ar

[1] Y. Tokura and N. Nagaosa, Science **288**, 462 (2000).
[2] J. B. Goodenough, *Magnetism and Chemical Bond* (Wiley, New York, 1963).
[3] N. Mufti, G. R. Blake, and T. T. M. Palstra, J. Magn. Magn. Mater. **321**, 1767 (2009).
[4] Y. Yamasaki, S. Miyasaka, Y. Kaneko, J.-P. He, T. Arima, and Y. Tokura, Phys. Rev. B **96**, 207204 (2006).
[5] S.-W. Cheong and M. Mostovoy, Nat. Mater. **6**, 13 (2007).
[6] M. Matsuda, H. Ueda, A. Kikkawa, Y. Tanaka, K. Katsumata, Y. Narumi, T. Inami, Y. Ueda, and S.-H. Lee, Nat. Phys. **3**, 397 (2007).
[7] Y. Tanaka, Y. Narumi, N. Terada, K. Katsumata, H. Ueda, U. Staub, K. Kindo, T. Kukui, T. Yamamoto, R. Kammuri, M. Hagiwara, A. Kikkawa, Y. Ueda, H. Toyokawa, T. Ishikawa, and H. Kitamura, J. Phys. Soc. Jpn. **76**, 043708 (2007).
[8] J. L. Dormann and M. Nogues, J. Phys.: Condens. Matter **2**, 1223 (1990).
[9] H. Martinho, N. O. Moreno, J. A. Sanjurjo, C. Rettori, A. J. García-Adeva, D. L. Huber, S. B. Oseroff, W. Ratcliff II, S.-W. Cheong, P. G. Pagliuso, J. L. Sarrao, and G. B. Martins, Phys. Rev. B **64**, 024408 (2001).
[10] A. J. García-Adeva and D. L. Huber, Phys. Rev. Lett. **85**, 4598 (2000).
[11] A. N. Yaresko, Phys. Rev. B **77**, 115106 (2008).
[12] K. Tomiyasu, J. Fukunaga, and H. Suzuki, Phys. Rev. B **70**, 214434 (2004).
[13] R. N. Bhowmik, R. Ranganathan, and R. Nagarajan, Phys. Rev. B **73**, 144413 (2006).
[14] S. Blanco-Canosa, F. Rivadulla, V. Pardo, D. Baldomir, J.-S. Zhou, M. García-Hernández, M. A. López-Quintela, J. Rivas, and J. B. Goodenough, Phys. Rev. Lett. **99**, 187201 (2007).
[15] M. Tovar, G. Alejandro, A. Butera, A. Caneiro, M. T. Causa, F. Prado, and R. D. Sánchez, Phys. Rev. B **60**, 10199 (1999).
[16] F. K. Lotgering, Philips Res. Rep. **11**, 190 (1956).
[17] E. Winkler, M. T. Causa, J. J. Neumeier, and S. B. Oseroff, J. Magn. Magn. Mater. **310**, e959 (2007).
[18] G. E. Pake and T. L. Estle, *The Physical Principles of Electron Paramagnetic Resonance* (W. A. Benjamin Inc., Massachusetts, 1973).
[19] J. M. Hastings and L. M. Corliss, Phys. Rev. **126**, 556 (1962).
[20] J. Samuel Smart, *Effective Field Theories of Magnetism* (W. B. Saunders Company, London, 1966).
[21] N. W. Ashcroft and N. D. Mermin, *Solid State Physics* (Saunders College, Philadelphia, 1976).
[22] K. Takubo, J.-Y. Son, T. Mizokawa, H. Ueda, M. Isobe, Y. Matsushita, and Y. Ueda, Phys. Rev. B **74**, 155103 (2006).
[23] K. Motida and S. Miyahara, J. Phys. Soc. Jpn. **28**, 1188 (1970).
[24] A. H. Morrish, *The Physical Principles of Magnetism* (IEEE Press, NY, 2001).
[25] N. Tristan, J. Hemberger, A. Krimmel, H.-A. Krug von Nidda, V. Tsurkan, and A. Loidl, Phys. Rev. B **72**, 174404 (2005).
[26] P. L. Edwards, Phys. Rev. **116**, 294 (1959).
[27] D. L. Huber, Phys. Rev. B **12**, 31 (1975).
[28] A. Abragam and B. Bleaney, *Electron Paramagnetic resonance of Transition Ions* (Dover Publications, Inc., NY, 1986).
[29] F. Rivadulla, M. A. López-Quintela, L. E. Hueso, J. Rivas, M. T. Causa, C. Ramos, R. D. Sánchez, and M. Tovar, Phys. Rev. B **60**, 11922 (1999).
[30] E. Winkler, M. T. Causa, and C. A. Ramos, Physica B **398**, 434 (2007).
[31] M. T. Causa, M. Tovar, A. Caneiro, F. Prado, G. Ibañez, C. A. Ramos, A. Butera, B. Alascio, X. Obradors, S. Piñol, F. Rivadulla, C. Vázquez-Vázquez, A. López-Quintela, J. Rivas, Y. Tokura, and S. B. Oseroff, Phys. Rev. B **58**, 3233 (1998).
[32] D. L. Huber, G. Alejandro, A. Caneiro, M. T. Causa, F. Prado, M. Tovar, and S. B. Oseroff, Phys. Rev. B **60**, 12155 (1999).
[33] G. Alejandro, M. C. G. Passeggi, D. Vega, C. A. Ramos, M. T. Causa, M. Tovar, and R. Senis, Phys. Rev. B **68**, 214429 (2003).
[34] T. G. Castner, Jr. and Mohindar S. Seehra, Phys. Rev. B **4**, 38 (1971).
[35] J. E. Gulley, Daniel Hone, D. J. Scalapino, and B. G. Silbernagel, Phys. Rev. B **1**, 1020 (1970).
[36] M. T. Causa and M. C. G. Passeggi, Phys. Lett. **98A**, 291 (1983).
[37] P. M. Raccah, R. J. Bouchard, and A. Wold, J. Appl. Phys. **37**, 1436 (1966).
[38] I. Saeki, T. Saito, R. Furuichi, H. Konno, T. Nakamura, K. Mabuchi, and M. Itoh, Corros. Sci. **40**, 1295 (1998).
[39] J. M. Recio, R. Franco, A. Martín Pendás, M. A. Blanco, L. Pueyo, and R. Pandey, Phys. Rev. B **63**, 184101 (2001).
[40] L. Gerward, J. Z. Jiang, J. Staun Olsen, J. M. Recio, and A. Waskowska, J. Alloys Compd. **401**, 11 (2005).
[41] I. M. Fita, R. Szymczak, M. Baran, V. Markovich, R. Puzniak, A. Wisniewski, S. V. Shiryaev, V. N. Varyukhin, and H. Szymczak, Phys. Rev. B **68**, 014436 (2003).
[42] A. Y. Ramos, H. C. N. Tolentino, N. M. Souza-Neto, J. P. Itié,

L. Morales, and A. Caneiro, Phys. Rev. B **75**, 052103 (2007).
[43] D. H. Lyons, T. A. Kaplan, K. Dwight, and N. Menyuk, Phys. Rev. **126**, 540 (1962).
[44] C. Ederer and M. Komelj, Phys. Rev. B **76**, 064409 (2007).
[45] F. Freyria Fava, I. Baraille, A. Lichanot, C. Larrieu, and R. Dovesi, J. Phys.: Condens. Matter **9**, 10715 (1997).
[46] J. Kanamori, in *Magnetism*, edited by G. T. Rado and H. Suhl (Academic Press, New York, 1963), Vol. I, Chap. 4, p. 127.